EPJ Web of Conferences **371**, 01007 (2026) https://doi.org/10.1051/epjconf/202637101007
AMT'2026

Study of a Rarefied Gas Driven by the Lid of a Micro cavity with a Diamond-Shaped Obstacle Using SRT-LBM

Yassine Bouhouchi[1*], *Meryem* Maiss[1], *Mohsine* Qaffou[1], *Youness* Ighris[1], *Brahim* Elaaddam[1], *Youssef* El Guennouni[2], *Jamal* Baliti[1], *Mohamed* Hssikou[1]

[1]Research team in Smart Electrical, Mechanical and Energy Systems (SEMES), Sultan Moulay Slimane University, Polydisciplinary Faculty, Beni Mellal, Morocco
[2]Moulay Ismail University, Faculty of Sciences, Meknes, Morocco

Abstract. The present study numerically investigates the flow and temperature behavior of a rarefied gas confined in a two-dimensional square lid-driven micro-cavity, with particular emphasis on the influence of a centrally located diamond-shaped obstacle. The upper wall moves at a constant velocity, while the bottom wall and the obstacle are heated, and the remaining walls are maintained at a lower temperature. Simulations are carried out using the lattice Boltzmann method, employing diffuse scattering boundary conditions at the moving lid and combined bounce-back-specular reflection scheme at the stationary walls and obstacle surfaces. Two configurations are examined: a cavity without an obstacle and a cavity containing a heated diamond-shaped obstacle. Rarefaction effects are analyzed over a range of Knudsen numbers, with a tangential momentum accommodation coefficient of $\sigma = 0.7$ .The results show that increasing rarefaction enhances velocity slip, reduces velocity amplitudes, and weakens vortical structures. While the obstacle strongly perturbs the flow at low Knudsen numbers, its influence progressively diminishes as rarefaction increases, leading to smoother velocity fields and reduced flow disturbances.

1 Introduction

Rarefied gas flows in microsocale and nanoscale geometries have received increasing attention due to their relevance in a broad range of applications, including micro electromechanical systems MEMS and nanoelectromechanical systems NEMS, vacuum technologies, and aerospace engineering [1]. At these scales, the continuum hypothesis gradually loses validity, and non-equilibrium effects become significant. The Knudsen number Kn, defined as the ratio of the molecular mean free path to a characteristic length scale, is the key parameter governing the degree of rarefaction. As Kn increases, classical Navier-Stokes-based models fail to accurately capture flow behavior, making alternative numerical approaches essential.

* Corresponding author: yassine.bouhouchi@usms.ac.ma

Lid-driven cavity flow has long been regarded as a canonical benchmark problem for investigating fluid dynamics in confined geometries. In the context of rarefied gas flows, this configuration has been extensively studied using particle-based and extended continuum methods. To et al. [2] employed molecular dynamics simulations to investigate pressure-driven flows between parallel plates using modified periodic boundary conditions. Hssikou et al. [3] applied the Direct Simulation Monte Carlo (DSMC) method to analyze two-dimensional dilute gas flow in a square cavity under gravity and thermal gradients, focusing on thermodynamic and transport properties. Mohammadzadeh et al. [4] compared monatomic and diatomic gas behavior in micro-and nanoscale lid-driven cavities using DSMC, highlighting differences in compressibility, vortex structures, and heat transfer. Mukherjee et al. [5] examined the influence of Knudsen number and lid velocity on flow rigidity and vortex dynamics in single and double lid –driven cavities. John et al. [6] studied no equilibrium flow and temperature transfer mechanisms in a lid driven cavity, revealing complex phenomena such as counter-gradient heat transfer at higher Kn. More recently, Baliti et al. [7] used the regularized 13-moment equations to assess the limits of the Navier-Stokes-Fourier framework and to capture rarefaction-induced non-classical effects. Despite these extensive investigations, most existing studies focus on simple cavity geometries without internal obstacles. However, the presence of solid obstacles is common in practical microscale devices and can significantly alter flow structure, vortex formation, and momentum transport, especially under rarefied conditions. The combined effects of rarefaction and complex internal geometries therefore remain insufficiently explored.

Among mesoscopic numerical approaches, the Lattice Boltzmann Method has emerged as a computationally efficient alternative for simulating gas flows. Its kinetic nature makes it particularly suitable for capturing non-equilibrium effects beyond the continuum regime. Nevertheless, accurate modelling of gas-surface interactions in LBM critically depends on the choice of boundary conditions. Commonly used schemes include bounce-back boundary conditions, specular reflection, hybrid bounce-back/specular models, and diffuse scattering boundary conditions [8]. The appropriate combination of these boundary conditions is essential to correctly represent momentum accommodation at solid surfaces, especially in slip and transition flow regimes. In this work, the Lattice Boltzmann method with a single-relaxation-time (SRT) collision model is employed to investigate rarefied gas flow in a lid-driven micro-cavity containing a diamond-shaped obstacle. Diffuse reflection boundary conditions are imposed on the moving lid, while specular reflection is applied to the fixed cavity walls and the obstacle surface. Simulations are performed over a range of Knudsen numbers spanning the slip and transition regimes. The study focuses on the influence of rarefaction on flow structure, vortex formation, and velocity distribution, as well as on the progressive attenuation of obstacle-induced flow disturbances with increasing Kn. By incorporating a non-trivial internal geometry, this work extends classical lid-driven cavity studies and provides new insights into rarefied gas dynamics in confined microscale systems.

2 Description of the geometry

The present study examines rarefied gas flow in a two-dimensional square micro-cavity of side length L=H, driven by the motion of the top wall, which moves horizontally at a constant velocity U_0, while the remaining walls are stationary. The bottom wall is uniformly heated and maintained at a constant dimensionless temperature θ_h, whereas the moving lid the vertical side walls are treated as cold isothermal boundaries. Two configurations are considered: a reference cavity without an internal obstacle (case 1) and a cavity containing a centrally located diamond-shaped obstacle maintained at the same temperature as the heated

bottom wall (case 2).This formulation enables a systematic assessment of the influence of internal solid structures on the flow and thermal characteristics under rarefied conditions.

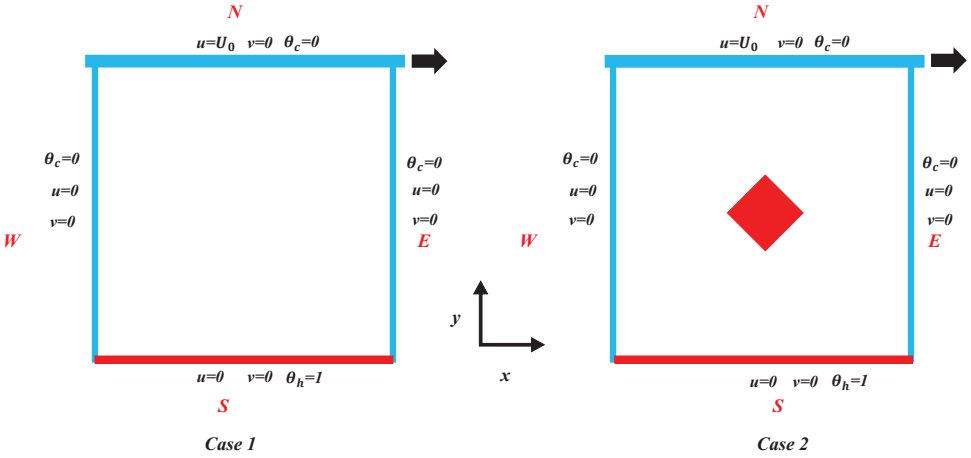

Fig. 1. Domain configuration.

3 Numerical Method

The Bhatnagar-Gross-Krook (BGK) [9] model as describes the governing equation for the distribution function:

$$f_k\left(x + v_{kx}.\Delta t, y + v_{ky}.\Delta t, t + \Delta t\right) - f_k(x, y, t) = \frac{-\Delta t}{\tau_f}\left[f_k(x, y, t) - f_k^{eq}{}_k(x, y, t)\right]. \quad (1)$$

Where τ_f represents the relaxation time for density and can be defined as the ratio of the mean free path λ to the mean thermal velocity:

$$\tau_f = \frac{\lambda}{\langle v \rangle} = \lambda\sqrt{\frac{\pi}{8RT}} \quad (2)$$

In the Lattice Boltzmann Method (LBM), $c = \sqrt{3RT} = 1$.
For the D_2Q_9 model, the Knudsen number, which quantifies the gas rarefaction, plays a key role in characterizing flows in microfluidic devices [10]:

$$\tau_f = \lambda\sqrt{\frac{3\pi}{8}} \cong K_n H. \quad (3)$$

The distribution function f_k^{eq} is written at the equilibrium state as:
The equilibrium distribution function f_k^{eq} is given by:

$$f_k^{eq} = \rho w_k\left[1 + 3\frac{c_k.v}{c^2} + \frac{9}{2}\frac{(c_k.v)^2}{c^4} - \frac{3}{2}\frac{v^2}{c^2}\right]. \quad (4)$$

For the model D_2Q_9, the velocitiesc_k:

$$c_k = \begin{cases} (0,0), \mathrm{k} = 0, \\ (\cos\theta_k, \sin\theta_k), \quad \theta_k = (k-1)\frac{\pi}{2}, k = 1 \ldots\ldots 4, \\ \sqrt{2}\,(\cos\theta_k, \sin\theta_k), \quad \theta_k = (k-5)\frac{\pi}{2} + \frac{\pi}{4}, k = 5 \ldots\ldots 8. \end{cases} \quad (5)$$

The corresponding weighting values w_k are:

$$w_k = \begin{cases} \frac{4}{9}, \mathrm{k} = 0, \\ \frac{1}{9}, k = 1-4, \\ \frac{1}{36}, k = 5-8. \end{cases} \quad (6)$$

The macroscopic flow quantities are defined as:

$$\rho(x,y,t) = \sum_{k=0}^{8} f_k(x,y,t), \quad (7)$$

$$\rho(x,y,t)u(x,y,t) = \sum_{k=1}^{9} v_k f_k(x,y,t), \quad (8)$$

4 Boundary Conditions

In this work, diffuse scattering boundary conditions are applied to the top wall, while a combination of bounce-back and specular reflection conditions (BSBC) are used at the walls of the obstacle and the fixed walls.

4.1 Diffuse scattering boundary conditions

At the top wall, moving with a horizontal velocity $u(U0, 0)$ (figure 1), the unknown distribution functions $f_4, f_7 and\ f_8$ are computed as follows [11]:

$$f_4 = \frac{A_n}{\rho_w} f_4^{eq}(f_2 + f_5 + f_6), \quad (9)$$

$$f_7 = \frac{A_n}{\rho_w} f_7^{eq}(f_2 + f_5 + f_6), \quad (10)$$

$$f_8 = \frac{A_n}{\rho_w} f_8^{eq}(f_2 + f_5 + f_6). \quad (11)$$

In the $\boldsymbol{D_2Q_9}$ model, the value of $\boldsymbol{A_n}$ is set to $\boldsymbol{6}$ [12].

4.2 Bounce-back and specular reflection conditions

The combination of bounce-back and specular reflection conditions is favored by the tangential momentum accommodation coefficient $\sigma\ (TMAC)$ expressed by the following relation [13]:

$$\sigma = \frac{M_i - M_r}{M_i - M_w}. \quad (12)$$

Where M_i, M_r and M_w represent the tangential moments of the incident, reflected, and wall associated molecules, respectively. This coefficient equals 0 for specular reflection and 1 for bounce-back.

At the bottom wall, the unknown distribution functions (f_2, f_5, f_6) are determined from the known distribution functions (f_4, f_7, f_8) by the following equations:

$$f_2 = f_4, \quad (13)$$

$$f_5 = \sigma f_7 + (1-\sigma) f_8, \quad (14)$$

$$f_6 = \sigma f_8 + (1-\sigma) f_7. \quad (15)$$

At the west wall, the unknown distribution functions (f_1, f_5, f_8) are determined from the known distribution functions (f_3, f_7, f_6) by the following equations:

$$f_1 = f_3, \quad (16)$$

$$f_5 = \sigma f_7 + (1-\sigma) f_6, \quad (17)$$
$$f_8 = \sigma f_6 + (1-\sigma) f_7. \quad (18)$$

At the east wall, the unknown distribution functions (f_3, f_6, f_7) are determined from the known distribution functions (f_1, f_8, f_5) by the following equations:

$$f_3 = f_1, \quad (19)$$
$$f_6 = \sigma f_8 + (1-\sigma) f_5, \quad (20)$$
$$f_7 = \sigma f_5 + (1-\sigma) f_8. \quad (21)$$

5 Results and discussion

This study examines the flow of a rarefied gas square micro-cavity driven by a moving lid with a constant velocity U_0=0.01.Simulations are then conducted for a lid-driven cavity flow with a diamond-shaped obstacle at its center. The tangential momentum accommodation coefficient (TMAC) is set to σ=0.7, consistent with existing literature [14].

5.1 Mesh independence study

The mesh selection is based on an initial simulation without an obstacle, using the SRT-LBM approach at a Knudsen number of $Kn = 0.01$.Figure2 shows the impact of mesh size on the horizontal and the vertical velocity component profiles. Based on these findings, a mesh size of 200×200 was chosen for the subsequent simulations.

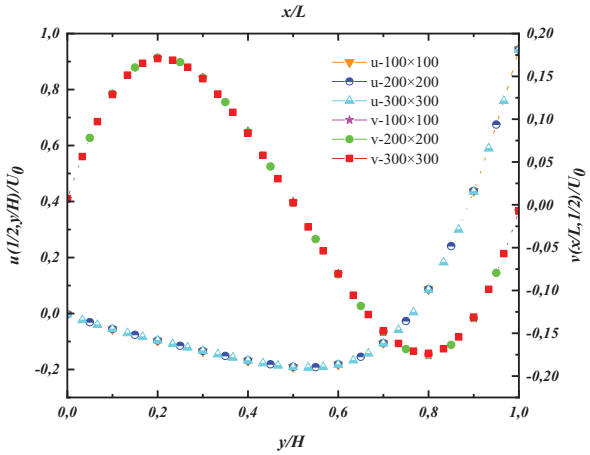

Fig. 2. Profiles of u/U_0 and v/U_0 for $Kn = 0.01$ obtained by the SRT-LBM method for different mesh grids.

5.2 Numerical Validation Test of the SRT-LBM

To validate the SRT-LBM model used in this study, Figure 4 compares the numerical solution profiles obtained using the SRT-LBM approach with those published by El Geunnouni [8], Perumal [14],and Rahmati [15] for Knudsen numbers $Kn = 0.01$ and $Kn = 0.1$. The comparison demonstrates that our results are in good agreement with the existing numerical solutions.

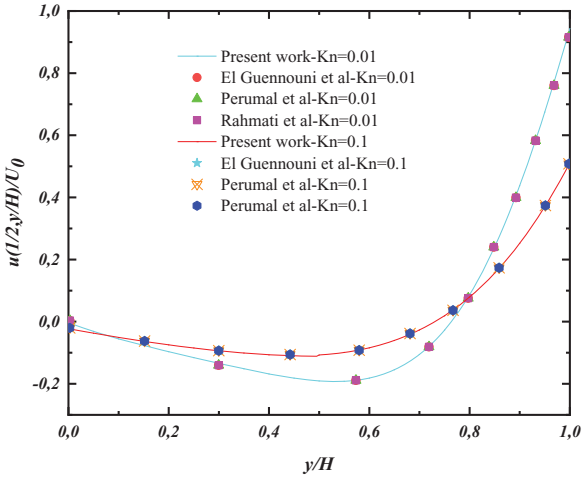

Fig. 3. Profiles of u/U_0 along x/L=0.5 line at $Kn = 0.01\ and\ 0.1$.

5.3 Numerical Results and Analysis

The horizontal velocity component u/U_0 is first examined along the vertical direction y/H in the absence of an obstacle (Fig. 4a). The profiles indicate that the flow is strongly influenced by the motion of the upper wall, which induces negative velocities over a large portion of the cavity $(y/H \leq 0.75)$ increases, a progressive rise in u/U_0 is observed , with the maximum value reached in the vicinity of the moving lid. The minimum velocity occurs for $Kn = 0.01$ at $y/H \approx 0.53$, close to the cavity center, reflecting a stronger momentum confinement under near-continuum conditions.

When a central obstacle is introduced (Fig. 4b), the velocity distribution is significantly altered. A large region of negative horizontal velocities develops below the obstacle, followed by a rapid increase in u/U_0 near the moving wall. The minimum value of the horizontal velocity is again observed for $Kn = 0.01$ at $y/H \approx 0.53$. The presence of the obstacle leads to a marked discontinuity in the velocity profiles, associated with the interruption and redistribution of the flow around the solid body. As the Knudsen number increases, slip effects at the walls become more pronounced, resulting in a systematic reduction of the velocity amplitudes. While slip remains weak at low Knudsen numbers, rarefaction effects become inceasingly significant at higher Kn values, strongly affecting the flow structure, particularly in the vicinity of the obstacle.

The variation of the vertical velocity component v/U_0 along the horizontal direction x/L in the absence of an obstacle is presented in Fig. 4c. The profiles exhibit a clear antisymmetric behavior, with positive values near $x/L \approx 0.2$ and negative values near $x/L \approx 0.8$, indicating a globally clockwise rotating flow induced by the moving lid. As the Knudsen number increases, rarefaction effects become more pronounced, leading to enhanced velocity slip at the walls and a progressive decrease in the amplitude of v/U_0. For $Kn = 0.01$, slip effects remain negligible,and the velocity at the moving wall satisfies $u(y = H) \approx U_0$, whereas non-equilibrium effects increasingly modify the flow behavior at higher Kn values.

In the presence of the central obstacle (Fig. 4d), the vertical profiles retain an overall antisymmetric structure, with positive values on the left side and negative values on the right side of the cavity. However, the obstacle introduces local disturbances in the flow field,

manifested by discontinuities and abrupt variations in v/U_0, which reflect the local perturbation and flow redistribution induces by the solid obstruction.

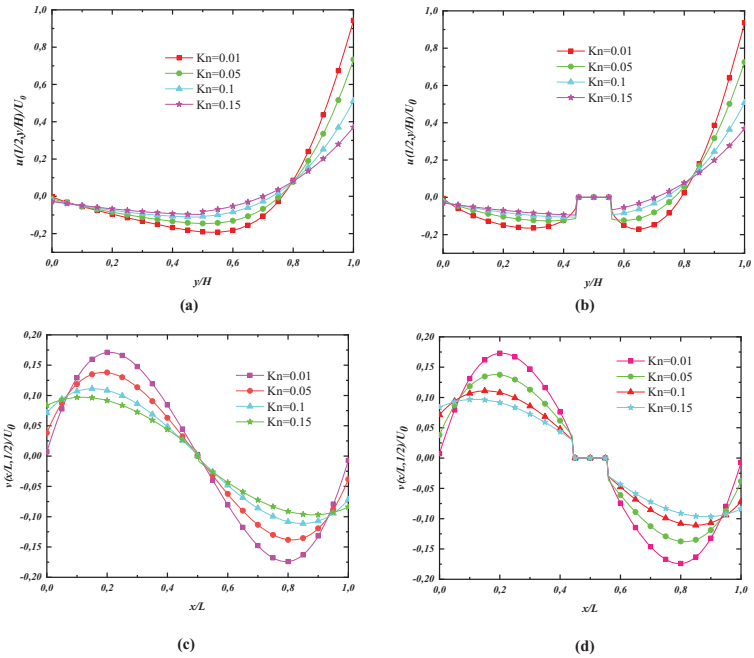

Fig. 4. Profiles of u-velocity components along the line x/H=1/2 (a) case (1) (b) case (2) and v-velocity components along the line y/H=1/2 (c) case (1) (d) case (2) for different Knudsen numbers.

Figures (5a-5d) illustrate the effect of the Knudsen number Kn on contours of the horizontal component u/U_0 of the veocity and the streamlines around an obstacle.When Kn is low ($Kn = 0.01$), the streamlines wrap strongly around the obstacle, forming symmetric vortices and a complex flow structure.

As Kn increases ($Kn = 0.05, Kn = 0.08$), the intensity of the vortices decreases, the streamlines are less deflected, and the perturbed zone reduces.

For higher values of Kn ($Kn = 0.1$), the vortices almost completely disappear, the streamlines follow the shape of the obstacle, and the flow perturbation becomes very weak.

In summary, as Kn increases, the influence of the obstacle on the streamlines decreases, the vortical structures weaken, and the perturbed zone reduces, showing a progressive adaptation of the streamlines to the cavity geometry.

Figures (6a-6d) show the evolution of vertical velocity contours around the obstacle as a function of the Knudsen number Kn. As Kn increases, a continuous decrease in the amplitude of vertical velocities, a progressive reduction of the zone influenced by the obstacle, a smoothing of velocity gradients and a homogenization of the velocity distribution are observed.

For low Kn values ($Kn = 0.01$), the contours show a strong vertical asymmetry with high vertical velocity values near the obstacle corners. In contrast, for higher Kn values ($Kn = 0.1$), the vertical velocities reach their lowest amplitude and the distribution becomes quasi-uniform in most of the domain.

These observations demonstrate that rarefaction effects progressively mitigate the influence of the obstacle on the vertical component of the flow, leading to an increasingly uniform velocity distribution.

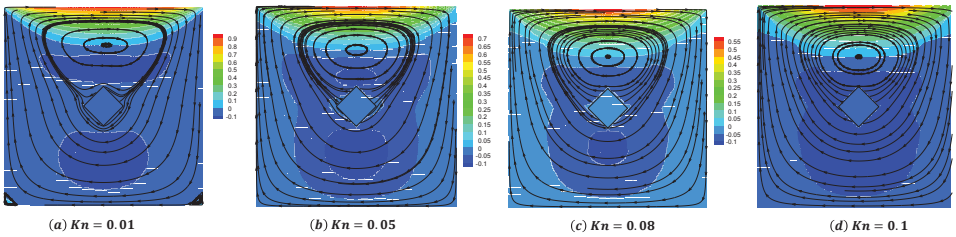

Fig. 5. Streamlines and u-velocity component obtained for different values of Kn in case 2.

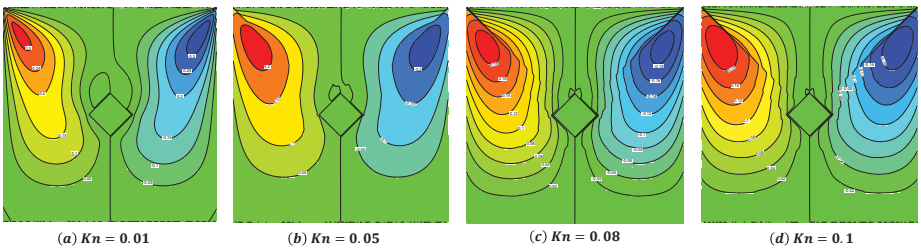

Fig. 6. Contours of v-velocity component obtained for different values of Kn in case 2.

The normalized temperature profiles along specific vertical lines within the micro-cavity are presented in Fig.7 and 8. In Fig. 7(a), the temperature θ along $x/L = 1/4$ is shown for different Knudsen numbers in case 2. As the Knudsen number increases from 0.01 to 0.1, the temperature gradient near the heated bottom wall decreases, and a pronounced temperature jump at the wall is observed, highlighting the significance of rarefaction effects and non-equilibrium transport. Fig. 7(b) illustrates the temperature along several vertical lines ($x/L = 1/4,1/3,1/2$) at $Kn = 0.01$, showing that the temperature decreases slightly faster toward the top wall at more central positions, reflecting lateral thermal diffusion within the cavity. In Fig. 8, a comparison between case 1 (no obstacle) and case 2 (with a centrally located diamond-shaped obstacle) along $x/L = 1/4$ reveals that the obstacle increases the local temperature in its vicinity,indicating that internal solid structures significantly affect the thermal distribution and impede vertical heat transport. These profiles demonstrate the interplay between rarefaction, thermal forcing, and internal obstacles on the cavity's temperature field.

The temperature contours presented in Fig.9 and 10 provide a two-dimensional visualization of these effects. In case2, Fig. 9 shows that at low $Kn(0.01)$, the contours are smooth and concentrated near the heated bottom wall, whereas increasing Kn leads to broader temperature distributions and enhanced wall temperature jumps.

The central diamond-shaped obstacle locally distorts the contours, creating steeper gradients and redistributing heat within the cavity. Fig. 10 compares case 1 and case 2 at $Kn = 0.01$, where the absence of an obstacle yields symmetric, vertically dominated heat transfer, while the presence of the obstacle modifies the flow, producing locally higher temperatures and altered thermal gradients.

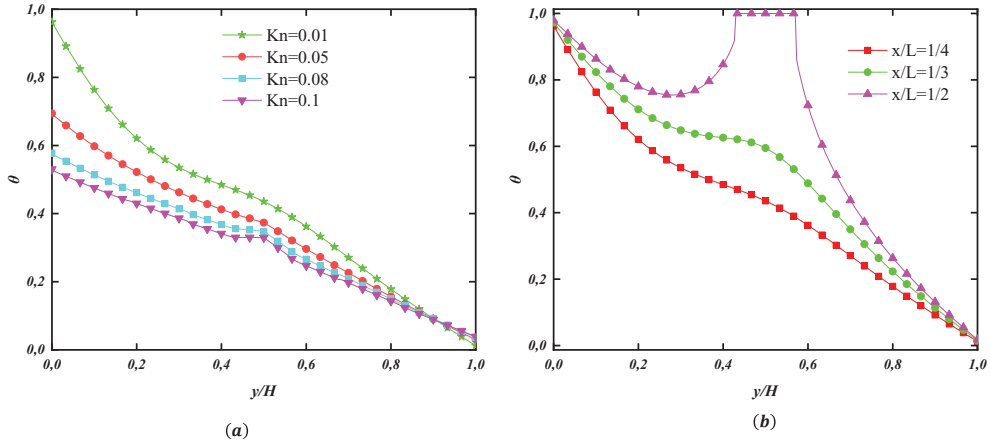

Fig. 7. (a) Normalized temperature along the $x/L = 1/4$ line for different Kn and (b) Normalized temperature in different x lines at $Kn = 0.01$ in case 2.

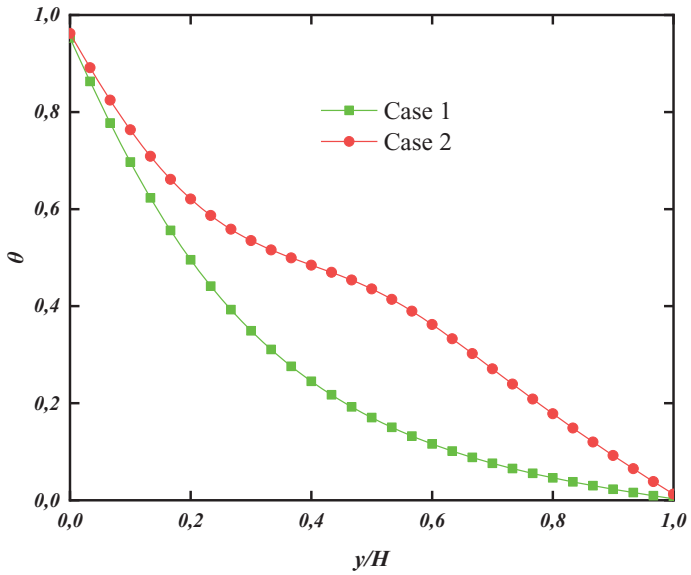

Fig. 8. Normalized temperature along the $X/L = 1/4$ line at $Kn = 0.01$ in both cases.

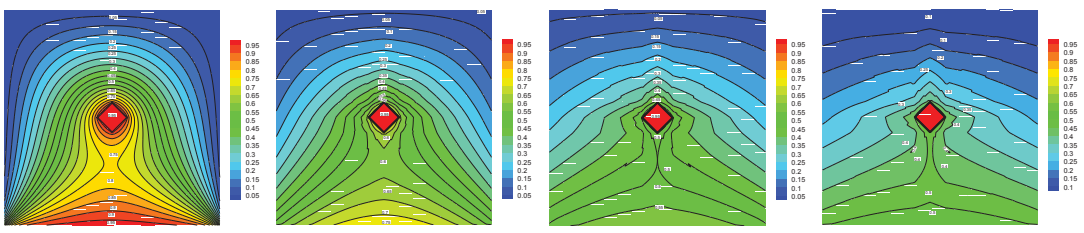

Fig. 9. Temperature contours for varying Kn in case 2.

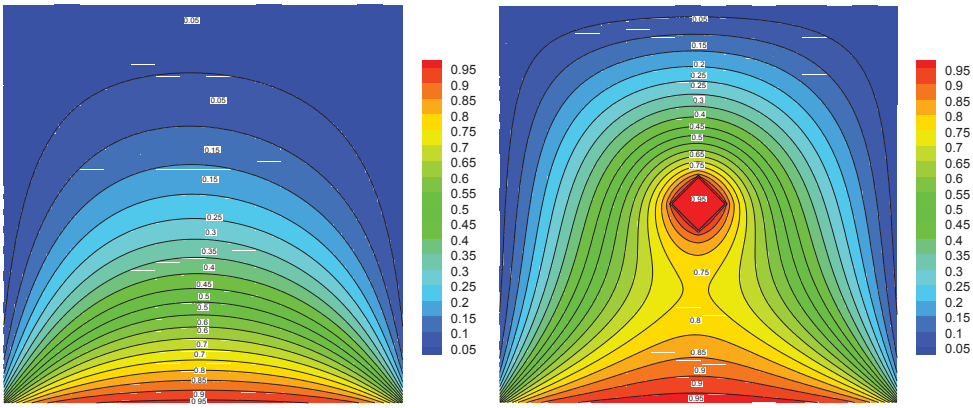

(***a***) ***Case* 1** (***b***) ***Case* 2**

Fig. 10. Temperature contours at $Kn = 0.01$ in both cases.

6 Conclusion

A numerical investigation of rarefied gas flow in a two-dimensional lid-driven square micro-cavity, with and without a centrally located diamond-shaped obstacle, has been performed using the lattice Boltzmann method. Diffuse scattering boundary conditions were applied at the moving lid, while combined bounce-back-specular reflection conditions were imposed on the stationary walls and obstacle surfaces. The influence of rarefaction was examined over a range of Knudsen numbers with a tangential momentum accommodation coefficient of σ = 0.7.

The results indicate that increasing rarefaction leads to enhanced velocity slip and a systematic reduction in velocity magnitudes. Vortical structures induced by the moving lid and the presence of the obstacle weaken progressively as the Knudsen number increases. At low Knudsen numbers, the obstacle significantly alters the flow fiels, generating strong local disturbances. At higher Knudsen numbers, these disturbances are attenuated, and the velocity field becomes smoother and uniform.

These results confirm that rarefaction effects reduce the influence of internal obstacles on the flow structure. The study emphasizes the necessity of incorporating appropriate gas-surface interaction models for accurate prediction of microscale flows with internal solid structures.

Nomenclature

A_n	Coefficient of normalization
c	Lattice speed
c_k	Lattice velocity vector
f_k, g_k	Density and temperature distribution function
f_{eq}, g_{eq}	Equilibrium density and temperature distribution function
H	Cavity height
K_n	Knudsen number
L	Cavity length
M	Tangential moments
R	Gas constant
r	Hexagonal obstacle radius

T	Gas temperature
t	Time
u	Velocity vector
U_0	Velocity of the moving wall
w_k	Weight factors in the equilibrium distribution

Greek Symbols

Δt	Time step
$\Delta x, \Delta y$	Lattice spacing in x and y directions
τ_f, τ_g	Relaxation times of density and internal energy functions
λ	Mean free path
ρ	Density
θ	Normalized temperature
σ	Tangential momentum accommodation coefficient

Acronyms

BGK	Bhatnagar-Gross-Krook
D_2Q_9	Lattice Boltzmann model
DSBCs	Diffuse scattering boundary conditions
DSMC	Direct Simulation Monte Carlo
LBM	Lattice Boltzmann method
MEMS	Micro-Electro-Mechanical systems
MRT	Multiple relaxation time
NEMS	Nano-Electro-Mechanical systems
R13	The regularized 13-moment
SBCs	Specular boundary conditions
SRT	Single relaxation time
TMAC	Tangential momentum accommodation

References

1. M. Gad-el Hak, The fluid mechanics of microdevices, Journal of Fluids Engineering, **121**, 5-33, (1999).
   https://doi.org/10.1115/1.2822013
2. Q. D. To, T. T. Pham, G. Lauriat and C. Léonard, Molecular Dynamics Simulations of Pressure-Driven Flows and Comparison with Acceleration-Driven Flows, Advances in Mechanical Engineering, **4**, 1-10, (2012).
   https://doi.org/10.1155/2012/580763
3. M. Hssikou, J. Baliti, Y. Bouzineb and M. Alaoui, DSMC method for a two-dimensional flow with a gravity field in a square cavity, De Gruyter, **21**, 59-67, (2015).
   https://doi:10.1515/mcma-2014-0009
4. A. Mohammadzadeh, E. Roohi and H. Niazmand, Simulation of Rarefied Gas Flow in Micro/Nano Cavity Using DSMC, the 10th Iranian Aerospace Society Conference, 1-8, (2011).
   http://irdoi.ir/807-307-389-731
5. S. Mukherjee, V. Shahabi, R. Gowtham, K. S. Rajan and R. K. Velamati, Effect of Knudsen Number Lid Velocity and Velocity Ratio on Flow Features of Single and

Double Lid Driven Cavities, Journal of Applied Fluid Mechanics, **12**, 1575-1583, (2019).
https://doi.org/10.29252/jafm.12.05.29335

6. B. John, X. J. Gu and D. R. Emerson, Investigation of heat and mass transfer in a lid-driven cavity under nonequilibrium flow conditions, Numerical Heat Transfer Part B, **58**, 287-303, (2010).
https://doi.org/10.1080/10407790.2010.528737
7. J. Baliti, M. Hssikou and M. Alaoui, Rarefaction and external force effects on gas microflow in a lid-driven cavity, Heat Transfer—Asian Res, **48**, 80-99, (2018).
https://doi.org/10.1002/htj.21369
8. Y. Elguennouni, M. Hssikou, J. Baliti, R. Ghafiri, and M. Alaoui, "SRT-LBM and MRT-LBM comparison for a lid-driven gas microflow" in 1st International Conference on Innovative Research in Applied Science, Engineering and Technology (IRASET), 1-6, IEEE, (2020).
https://doi.org/10.1109/IRASET48871.2020.9092233
9. P. L. Bhatnagar, E. P. Gross, and M. Krook, A model for collision processes in gases. I. small amplitude processes in charged and neutral one-component systems, Physical review, **94**, 511, (1954).
https://doi.org/10.1103/PhysRev.94.511
10. C. Lim, C. Shu, X. Niu, and Y. Chew, Application of lattice Boltzmann method to simulate microchannel flows, Physics of fluids, **14**, 2299-2308, (2002).
https://doi.org/10.18869/acadpub.jcme.34.1.97
11. S. Ansumali and I. V. Karlin, Kinetic boundary conditions in the lattice Boltzmann method, Physical Review E, **66**, 026311, (2002).
https://doi.org/10.48550/arXiv.nlin/0206033
12. X. Niu, C. Shu, and Y. Chew, Numerical simulation of isothermal micro flows by lattice Boltzmann method and theoretical analysis of the diffuse scattering boundary condition, International Journal of Modern Physics C, **16**, 1927-1941, (2005).
https://doi.org/10.1142/S0129183105008448
13. Y. H. Zhang, R. S. Qin, Y. H. Sun, R. W. Barber and D. R. Emerson, Gas Flow in Microchannels - A Lattice Boltzmann Method Approach, Journal of Statistical Physics, **121**, 257-267, (2005).
https://doi.org/10.1007/s10955-005-8416-9
14. D. A. Perumal, V. Krishna, G. Sarvesh and A. K. Dass, Numerical Simulation of Gaseous Microflows by Lattice Boltzmann Method, International Journal on Production and Industrial Engineering, **2**, 11-15, (2011).
https://doi: 10.5402/2012/630801
15. A. Rahmati, S. Niazi, A multi relaxation time lattice Boltzmann method for simulation of flow in micro devices, Proceedings of the 19th Annual Int. Conf. on Mechanical Engineering, Birjand, Iran, May (2011).